minerals

MDPI

Article

The Role of Mg Doping in Manipulating the Adsorption Mechanisms of CaAl-Layered Double Hydroxide: Investigating the Effects of Calcination Temperature and Borate Concentration Changes

Shuang Xu [1], Binling Guo [2,3], Keiko Sasaki [4] and Xinhong Qiu [1,*]

[1] School of Chemistry and Environmental Engineering, Wuhan Institute of Technology, Wuhan 430205, China; xushuang_0626@163.com
[2] School of Civil Engineering, Hefei University of Technology, Hefei 230009, China; gabriel116329@hotmail.com
[3] Engineering Research Center of Low-Carbon Technology and Equipment for Cement-Based Materials, Ministry of Education, Hefei 230009, China
[4] Department of Earth Resources Engineering, Kyushu University, Fukuoka 8190395, Japan; keikos@mine.kyushu-u.ac.jp
* Correspondence: qxinhong@gmail.com or qiuxh@wit.edu.cn

Abstract: CaAl-layered double hydroxides (LDHs) exhibit different mechanisms of borate removal at varying calcination temperatures. The addition of Mg alters the structure and composition of the calcined products, ultimately impacting their adsorption process. To investigate this, CaAl-LDH and Mg-doped CaAl-LDH with and without different calcination temperatures (500 °C and 900 °C) were prepared to immobilize a wide concentration range of borate. XRD, SEM, FTIR, and EXAFS techniques were employed to study the influence of Mg doping. The results indicate that the doping of Mg increases the BET surface area and enhances the adsorption capacity of uncalcined LDHs, with the enhancement being more pronounced at high borate concentrations. For LDHs calcined at 500 °C, Mg-doped LDHs exhibited slightly better adsorption at any borate concentration due to its more favorable ettringite formation. However, for LDHs calcined at 900 °C, Mg-doped LDHs (LDO) had a slightly better adsorption effect at low borate concentrations. At high concentrations, the crystallinity and morphology of the regenerated CaMgAl-LDH deteriorated, resulting in poor adsorption effects. These findings provide valuable theoretical support for understanding the mechanisms of removing pollutants with different concentrations by different LDHs.

Keywords: CaAl-LDH; Mg-doped; calcination; borate; initial concentration; mechanism

Citation: Xu, S.; Guo, B.; Sasaki, K.; Qiu, X. The Role of Mg Doping in Manipulating the Adsorption Mechanisms of CaAl-Layered Double Hydroxide: Investigating the Effects of Calcination Temperature and Borate Concentration Changes. *Minerals* **2023**, *13*, 1398. https://doi.org/10.3390/min13111398

Academic Editor: Raúl Fernández

Received: 20 September 2023
Revised: 17 October 2023
Accepted: 28 October 2023
Published: 31 October 2023

1. Introduction

Layered double hydroxides (LDHs) are a type of two-dimensional layered material that has been widely applied to pollutant adsorption [1,2]. LDHs are composed of positively charged brucite-like sheets containing intercalated anions in the hydrated interlayer region to balance positive charges. The general formula is: $M^{2+}_{1-x}M^{3+}_{x}(OH)_2]^{x+}[(A^{n-})_{x/n}\cdot yH_2O$, where M^{2+} and M^{3+} denote divalent and trivalent metal ions, respectively, A represents the interlayer anion, and x is the molar ratio of $M^{2+}/(M^{2+} + M^{3+})$ [3,4]. Of all the types of LDHs, Ca-based LDHs are distinctive because they are partially soluble in aqueous solution. This property enhances their removal efficiency and widens their applications [5,6], and several adsorption modes have been demonstrated for them [7]. Therefore, Ca-based LDHs are the focus of this paper.

The study of multi-component LDHs, synthesized by doping binary LDHs with other metals, has gained significant interest in recent years. Ce-doped ZnAl-LDH, for example, has shown higher separation efficiency of electrons and holes, resulting in enhanced photocatalytic activity compared to undoped ZnAl-LDH [8]. Wand et al. have reported that

ternary LDHs exhibit different morphologies with higher BET surface areas than binary LDHs, indicating increased adsorption capacity [9]. Mg and Ca are commonly associated elements in many substances. For instance, dolomite [$CaMg(CO_3)_2$] is a source of divalent metals (Mg^{2+}, Ca^{2+}) to synthesize MgAl-LDHs or CaMgAl-LDH [10–12]. Coal fly ash (CFA) and bottom ash, two main byproducts of coal combustion [13], can produce CaAl-LDH and MgAl-LDH when they contact with water [14,15]. Therefore, it is necessary to consider the effect of Mg doping on the properties of Ca-based LDHs.

Currently, some studies have demonstrated that the presence of Mg can alter the physicochemical properties of Ca-based LDHs. Ashekuzzaman et al. observed that adding both Ca and Mg as divalent precursors during synthesis improved the desorption-regeneration performance of Ca-based LDHs, as seen in CaMg-based LDHs [16]. However, the impact of Mg doping on the adsorption process and mechanism of Ca-based LDHs has not been thoroughly investigated. Further research into this area is crucial to gain a deeper understanding of the adsorption properties of Ca-based LDHs.

Moreover, we have discovered that the concentration of pollutants has a significant impact on the adsorption mechanism of CaAl-LDH and CaMgAl-LDH [17]. Utilizing various characterization techniques, we have identified at least three adsorption mechanisms of arsenate by these two LDHs: the intercalation, dissolution-reprecipitation (DR) reaction and surface complexation. We have also observed notable differences in adsorption efficiencies and mechanisms between CaAl-LDH and Mg-doped CaAl-LDH, with the DR mechanism playing a crucial role in elucidating these variations. While we confirmed some important conclusions, we have yet to explore in detail the structural changes of LDHs after Mg doping, nor have we investigated the effects of different calcination temperatures on the properties of these materials.

Calcination has a significant impact on the structure and composition of LDHs and greatly enhances their adsorption performance. Notably, unlike MgAl-LDH, which can restore its original layer structure after calcination, CaAl-LDH produces different calcined products at varying temperatures, leading to distinct adsorption processes [11]. For instance, when borate is adsorbed onto CaAl-LDH calcined at 300 °C or 500 °C, it forms borate-containing ettringite; however, when calcined at 900 °C, the boron species adsorbed on the alumina gel created from the hydration of $Ca_{12}Al_{14}O_{33}$, then immobilized as HBO_3^{2-} into the interlayer of new LDHs. Furthermore, Suleiman compared the removal efficacy of pristine and calcined ZnAl-, MgAl-, and ZnMgAl-LDHs, revealing that the pristine ZnMgAl-LDH had the worst adsorption results, but exhibited the best adsorption efficiency after calcination [18]. This suggests that calcination can significantly enhance the adsorption efficiency of Mg-doped LDHs. However, there are currently limited reports on the effect of calcination temperatures on the adsorption of Mg-doped CaAl-LDH.

As an anionic pollutant, borate is special for LDHs. It has multiple forms in an aqueous solution and the different types of LDHs show various adsorption modes for them [19,20]. Therefore, this study used borate as a model anion. To explore the effect of Mg doping on the adsorption mechanism of borate by CaAl-LDH with various calcination temperatures, several characterization techniques were utilized, including XRD, TG, SEM, FTIR, and EXAFS. Additionally, the adsorption mechanisms are believed to depend on the borate concentration, so a wide range of borate concentrations was examined in the present study. This research builds upon our understanding of borate immobilization on Ca-based LDHs and may provide insight into the adsorption behavior of binary and ternary metallic LDHs under different aqueous systems.

2. Experimental Method

2.1. Preparation of LDHs and Calcined LDHs

The synthesis of CaAl-LDH and CaMgAl-LDH was carried out according to the method in our previous work [17,21]. The preparation of different LDHs was described in detail in Supplementary Materials Test S1. Before sorption experiments, some LDHs were

calcined for 3 h at 500 °C and 900 °C, respectively, and the calcined products were named CaAl-500, CaAl-900, CaMgAl-500 and CaMgAl-900.

2.2. Sorption Experiments

2.5 mmol L^{-1} (154.6 mg L^{-1}) borate solution with pH = 7 for the timeline experiment was prepared. Firstly, 0.100 g of adsorbent was added to a centrifuge tube with 40 mL of borate solution, followed by shaking at 100 rpm at room temperature using a shaking incubator. After a certain time of reaction, the centrifuge tube was taken out, and the solution was filtered by a 0.45 μm membrane filter. The supernatant liquor was analyzed boron concentration using azomethine-H hydrates color-developing agent in UV-VIS spectrophotometer at 420 nm, and the solid residue was collected for further characterization.

Then we explored the effect of different concentrations of borate. Due to high concentrations of H_3BO_3 (>25 mM) in solution could form a polymeric state, so 0.1, 0.8, 2.5, 5, 10, 15, and 20 mmol L^{-1} borate solutions were prepared. The adsorption procedure was in the same manner as above. But the reaction time is only 48 h. Then the filtered supernatants were collected for determination of total concentrations of B, and the solid residues after sorption were also collected for further characterization. See Supplementary Materials Test S2 for specific information on characterization techniques.

3. Results

3.1. The Effect of Mg Doping on CaAl-LDH with Different Calcination Temperatures

3.1.1. The Change of Adsorption Capacity and pH

The influence of Mg doping on the adsorption of 2.5 mM borate on CaAl-LDH with different calcination temperatures was first discussed.

The change of B concentration and pH in solution over reaction time is shown in Figure 1a. As the calcination temperature increased, the borate removal was better. The doping of Mg improved the removal effect, except for CaMgAl-900, but it was litter better at the end of the reaction. This indicated that the doping of Mg has different effects on the adsorption of different calcined CaAl-LDHs. Simultaneously, changes in the pH of the solution are shown in Figure 1b. The pH values of the solution immediately increased to about 12 and reached equilibrium. This is due to Ca-based LDHs being alkaline material and could release a large amount of OH^- when dissolved in solution. In order to ensure the structural stability of LDH, pH during the reaction was not adjusted.

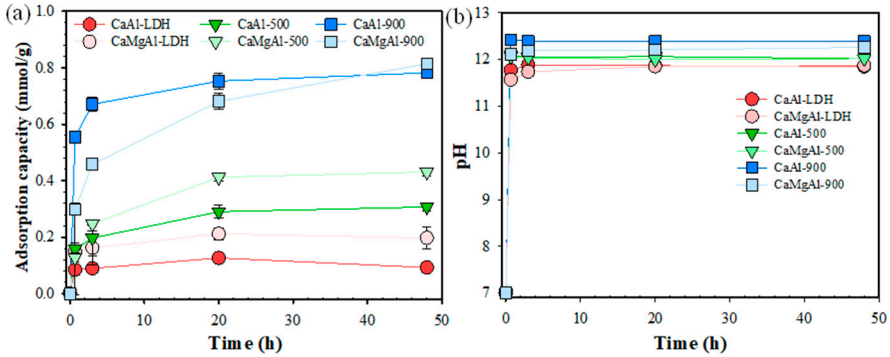

Figure 1. Changes of B concentration (**a**), pH (**b**) during sorption of 2.5 mM B in CaAl-LDH, CaAl-500, CaAl-900 and in CaMgAl-LDH, CaMgAl-500, CaMgAl-900.

3.1.2. Adsorption Kinetic

The kinetic mechanism of borate adsorption was studied using two different models: Pseudo-first-order (Equation (1)) and Pseudo-second-order kinetic model (Equation (2)). The two kinetic models are expressed as follows:

$$Q_t = Q_e\left(1 - e^{-k_1 t}\right) \quad (1)$$

$$\frac{t}{Q_t} = \frac{1}{k_2 {Q_e}^2} + \frac{t}{Q_e} \quad (2)$$

The amounts adsorbed at equilibrium (Q_e, mmol/g) and at various times t (h) (Q_t, mmol/g), and the rate constants of a pseudo-first-order kinetic model (k_1, h^{-1}) and pseudo-second-order kinetic model (k_2, g/mmol h).

The linear fitting diagrams for both adsorption kinetic models were presented in Figure S1, and the relevant parameters were summarized in Table 1. Comparing the correlation coefficient (R^2) of the two models, it was found that the pseudo-second-order model could more accurately describe the adsorption kinetic behavior of these materials. This indicated that the adsorption rate depends more on the active sites of the adsorbent surface [22]. Furthermore, the Q_e values of different Mg-doped adsorbents were larger than the corresponding CaAl-LDH, indicating that Mg doping improved the adsorption performance of binary LDHs.

Table 1. The kinetics model parameters for borate adsorption.

Adsorbent	Pseudo-First-Order			Pseudo-Second-Order		
	Q_e (mmol/g)	k_1 (1/h)	R^2	Q_e (mmol/g)	k_2 (g/(mmol h)	R^2
CaAl-LDH	0.1029	2.5434	0.9057	0.0944	0.0731	0.9863
CaAl-500	0.2804	0.8094	0.9041	0.3111	0.2765	0.9988
CaAl-900	0.7369	2.0659	0.9843	0.7849	0.2778	0.9997
CaMgAl-LDH	0.1909	2.2327	0.9554	0.1996	0.0109	0.9987
CaMgAl-500	0.4196	0.3387	0.9824	0.4417	0.5873	0.9982
CaMgAl-900	0.7374	0.4187	0.9327	0.8243	1.3792	0.9934

3.1.3. Thermal Analysis (TGA and DSC)

To investigate the thermal behaviors of two types of LDHs, thermos-gravimetric analysis (TGA) and differential scanning calorimetry (DSC) were carried out, as shown in Figure S2. The TGA-DSC curves showed three main weight loss stages for both CaAl-LDH and CaMgAl-LDH.

Firstly, 9.5% and 10.61% weight loss from room temperature to 200 °C assigned to the evaporation of adsorbed water and interlayer water in CaAl-LDH and CaMgAl-LDH. Secondly, 14.39% and 16.55% weight loss from 200 °C to 410 °C corresponded to the simultaneous elimination of intercalated NO_3^- and structural water, as well as the dehydration of the brucite-like octahedral layers in CaAl-LDH and CaMgAl-LDH [23]. Lastly, 12.99% and 13.34% weight loss from 410 °C to 620 °C was attributed to partial decarbonization and further decomposition in CaAl-LDH and CaMgAl-LDH [24]. Based on the above results, it can be seen that CaMgAl-LDH had a greater mass loss. Firstly, since the atomic radius of Mg is smaller than that of Ca, the doping of Mg could affect the arrangement structure of the original CaAl-LDH and reduce the stability. Secondly, compared with Ca, Mg has a weaker metallicity, so the Mg-O bond is more easily damaged. Therefore, the results of TG-DSC revealed that the doping of Mg affected the stability of CaAl-LDH, making it more susceptible to temperature.

3.1.4. Brunauer-Emmett-Teller (BET) Surface Area Analysis

To acquire the specific surface areas and pore structure characteristics of different adsorbents, N_2 adsorption-desorption experiments were conducted, as shown in Figure S3. As can be seen, the N_2 adsorption-desorption isotherm of these materials has a type-IV isotherm shape with an H3-type hysteresis loop, indicating a mesoporous structure for LDHs [22]. Relevant data can be found in Table S1. After calcination, the surface area increased due to the removal of water and NO_3^- molecules from the LDH crystal. Moreover, Mg doping was found to increase the BET surface area, total pore volume and pore size of CaAl-LDH with different calcination temperatures. The surface area was an

essential quantitative indicator of borate removal performance by the adsorbent, as it plays a vital role in the kinetics of solid-liquid reactions [25].

3.1.5. Crystal Structure Analysis

The changes in XRD patterns for these materials during the reaction are presented in Figure 2. The XRD pattern of CaAl-LDH and CaMgAl-LDH obviously showed a crystal structure of LDHs (Figure 2a,d) [26,27]. After 20 min of adsorption, two types of LDHs with an interlayer spacing of 8.52 Å for NO_3^- and 7.56 Å for OH^- as interlayer anions appeared [28]. However, the peak intensity of CaMgAl-LDH with interlayer spacing of 7.56 Å was obviously greater. Especially at 48 h, the interlayer spacing of CaMgAl-LDH is only 7.56 Å. This might suggest that the doping of Mg facilitated the ion exchange of NO_3^- with OH^-. This also suggested that their adsorption mechanism of borate was not ion exchange.

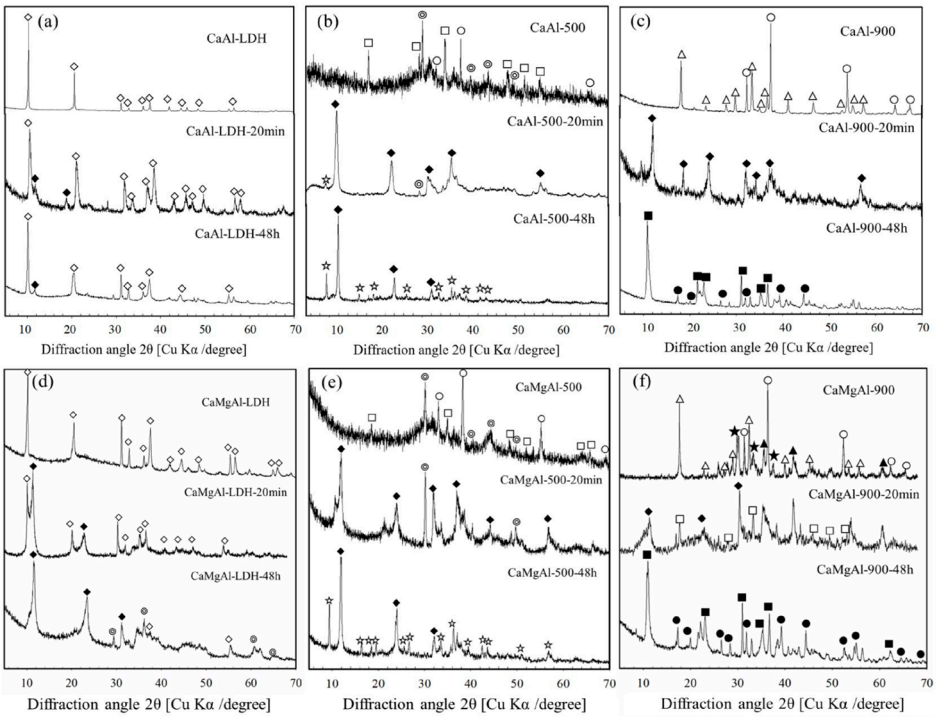

Figure 2. XRD patterns of the solid residues before and after sorption of 2.5 mM B. (**a**) CaAl-LDH, and after 20 min and 48 h of adsorption, (**b**) CaAl-500, and after 20 min and 48 h of adsorption, (**c**) CaAl-900, and after 20 min and 48 h of adsorption, (**d**) CaMgAl-LDH, and after 20 min and 48 h of adsorption, (**e**) CaMgAl-500, and after 20 min and 48 h of adsorption, (**f**) CaMgAl-900, and after 20 min and 48 h of adsorption. Symbols: ◇, CaAl-LDH/CaMgAl-LDH (interlayer anion: NO_3^-); ◆, Ca(Mg)Al-LDH (interlayer anion: OH^-); ☆, borate-containing ettringite ($Ca_6[Al(OH)_6]_2[B(OH)_4]_6$); △, $Ca_{12}Al_{14}O_{33}$; ■, Ca-Al-LDH (interlayer anion: $B(OH)_4^-$); ◎, $CaCO_3$; □, $Ca(OH)_2$; ○, CaO; ▲, MgO; ★, $Ca_5Al_6O_{14}$; •, $Ca_3Al_2(OH)_{12}$.

After calcination at 500 °C the original layer structure of LDHs was completed, destroyed and transformed into a mixture of CaO, $Ca(OH)_2$, and $CaCO_3$ (Figure 2b,e). After adsorption, both CaAl-500 and CaMgAl-500 were restored to their original layered structure. Ettringite appeared earlier in the CaAl-500 system, but the relative content of ettringite in the CaMgAl-500 system was higher at the end of the reaction. In addition, the crystallinity of the regenerated product in the CaMgAl-500 system was poor. The results indicated that the presence of Mg inhibits the regeneration of CaMgAl-500 but favored the structural transformation of LDHs to ettringite, while the formation of borate-containing ettringite was the main reason for the removal of borate [11].

When the calcination temperature reached 900 °C a new crystal phase ($Ca_{12}Al_{14}O_{33}$) appeared in the calcined product (Figure 2c,f). Moreover, a small amount of MgO existed in the CaMgAl-900 system. After adsorption for 20 min, CaAl-900 was regenerated into LDHs with poor crystallinity, but CaMgAl-900 was not fully regenerated, some $Ca(OH)_2$ was still present, indicating that the structural transformation (or regeneration) of CaMgAl-900 was slower. After 48 h, the solid residue consisted of LDHs with an interlayer spacing of 8.12 Å and new crystalline phases ($Ca_3Al_2(OH)_{12}$). The peak intensity of them in the CaMgAl-900 system was stronger.

3.1.6. Extended X-ray Absorption Fine Structure Analysis

For the seven samples and the related standard $Ca(OH)_2$, Ca K-edge XANES spectra (Figure 3a) the FT k^3-weighted EXAFS spectra (Figure 3b) were collected. Firstly, there was a weak pre-edge feature at ~4040 eV corresponding to transitions from 1s to 3d state (Figure 3a) [29], which indicates the distorted 7-fold Ca-OH with a low structural symmetry existing in Ca-containing LDHs [30]. Therefore, it cannot be found in the $Ca(OH)_2$ standard with a symmetric octahedron. But for CaMgAl-900 and CaAl-900, their pre-edge features were not obvious, probably because the main component of the two samples was $Ca_{12}Al_{14}O_{33}$. However, they showed another peak at ~4046 eV, as was observed in the XANES region of $Ca(OH)_2$. In addition, the other peak presented in other samples (~4051 eV) was lower than that of the calcium hydroxide reference (~4053 eV), which suggested a decreased average oxidation state of Ca^{2+} in these samples [31].

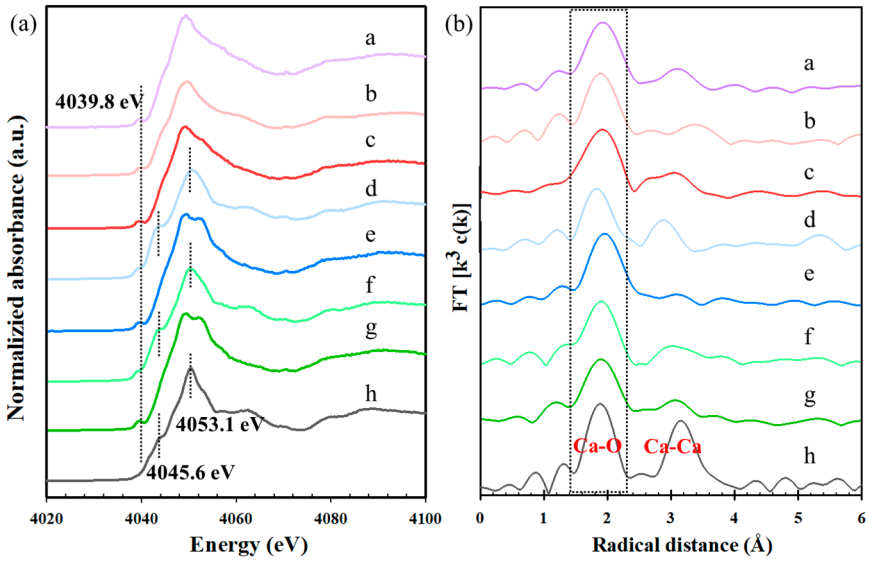

Figure 3. Normalized XANES spectra (**a**) and Fourier-transform EXAFS spectra (**b**) at Ca K-edge for different samples. a: CaMgAl-LDH-2.5 mM, b: CaMgAl-500, c: CaMgAl-500-2.5 mM, d: CaMgAl-900, e: CaMgAl-900-2.5 mM, f: CaAl-900, g: CaAl-900-2.5 mM, h: $Ca(OH)_2$.

In Fourier transform EXAFS spectra at the Ca K-edge (Figure 3b), for the result of $Ca(OH)_2$, the magnitude exhibited two strong peaks which represented the atomic distance of Ca−O at 1.87 Å and the atomic distance of Ca−Ca at 3.12 Å [32]. In addition, for all samples, there was a noticeable change in the peak of Ca−Ca. The fitting results including coordination number, bond distance, and Debye–Waller factor are listed in Table 2. The different coordination numbers and interatomic distances of the Mg-doped LDHs demonstrated that the presence of Mg had different effects on the Ca-LDHs with different calcination temperatures. Among them, the Ca−O distance in CaMgAl-900-2.5 mM (2.44 Å) was litter longer than that in CaAl-900-2.5 mM (2.42 Å), indicating a lattice expansion of Ca−O−Mg octahedron. This lattice expansion induced an enhanced exposure of Ca^{2+} s-orbital and thus strengthened the interaction between Ca^{2+} and the 7-fold OH^- (OH^- group as an electron donor), which increased the average electron density of Ca

ions [30]. However, comparing the above result, the local fine structure around Ca^{2+} was not significantly affected by the presence of Mg^{2+}.

Table 2. Ca K-edge EXAFS fitting results of various samples.

Sample	Shell	CN	R (Å)	σ^2	Rf (%)
a CaMgAl-LDH-2.5 mM	Ca-O	6.18	2.41	0.009	2.1
b CaMgAl-500	Ca-O	4.66	2.39	0.009	4.6
c CaMgAl-500-2.5 mM	Ca-O	6.18	2.39	0.009	3.6
d CaMgAl-900	Ca-O	4.65	2.34	0.008	4.6
e CaMgAl-900-2.5 mM	Ca-O	6.06	2.44	0.009	3.1
f CaAl-900	Ca-O	4.16	2.37	0.007	2.1
g CaAl-900-2.5 mM	Ca-O	6.06	2.42	0.009	2.5
h $Ca(OH)_2$ std	Ca-O	6.00	2.36	0.008	4.7

Coordination number (CN), interatomic distance (R), Debye-Waller factor (σ^2), and residual factor (Rf).

3.1.7. FTIR Analysis after Adsorption

In addition, the FTIR spectra of solid residues after adsorption are supplied in Figure S4. Regarding CaAl-LDH, the calcination did not affect the FTIR spectra. All of them had typically board bands in the range of 3400–3600 cm^{-1} and a peak at around 1623 cm^{-1}, which are associated with the stretching bands of the hydrogen-bonded hydroxyl groups and H_2O from both the surface and interlayer of LDHs [33]. However, for uncalcined LDHs, according to the XRD result (Figure 2), the values of the interlayer spacing were 8.52 and 7.56 Å, indicating that the interlayer anions were NO_3^- and OH^-. Therefore, the absorption peak at 1390 cm^{-1} belongs to the characteristic band of N-O [34]. For LDHs calcined at 500 °C, CO_3^{2-} present in the solution was mainly reacted with Ca^{2+} that was released from the material to generate $CaCO_3$. The absorption peak at about 1390 cm^{-1} belongs to the characteristic band of C-O. For LDHs calcined at 900 °C according to the XRD result (Figure 2), the value of the interlayer spacing was 8.12 Å, indicating that the interlayer anion was not NO_3^-. So, the vibration peak around 1380 cm^{-1} corresponded to CO_3^{2-}. However, CO_3^{2-} in the interlayer of LDHs can very easily be replaced by other anions. The sharp peaks at around 1400 cm^{-1} and 1060 cm^{-1} are assigned to monodentate carbonate [34]. The peaks in the range of 400 to 800 cm^{-1} are originated from metal-oxygen vibrations. The stretching and deformation vibrations of Al–OH can be observed at 788 cm^{-1}, whereas the broad bands at 535 cm^{-1} and 425 cm^{-1} are attributed to those of Ca–OH, Ca–O–Ca, and O–Ca–O bonds [23]. The Mg-doped adsorbents after the reaction also had similar results, except that the peaks at 785, 670 and 540 cm^{-1} belonged to M-O stretching and M-O-M bending modes, (M=Mg, Al) [35].

3.2. The Effect of Different Borate Concentrations

According to previous research [17], the initial concentration of arsenate had a different impact on the adsorption of CaAl-LDH and CaMgAl-LDH, causing different removal mechanisms at different concentration ranges. Therefore, in addition to investigating the effect of initial borate concentrations on CaAl-LDH with different calcination temperatures, it is more important to explore the influence of Mg doping on these processes.

3.2.1. The Change of Equilibrium Adsorption Capacity

The equilibrium adsorption capacities (Q_e) of borate by CaAl-LDH and CaMgAl-LDH with different calcination temperatures in a wide borate concentration are shown in Figure 4. For Figure 4a, the Mg-doped LDHs presented greater adsorption capacities, especially in a high concentration range (10–20 mM). After calcination at 500 °C (Figure 4b), the adsorption capacity of CaMgAl-500 was slightly higher than that of CaAl-500 at any borate concentrations. But at low concentrations (0.1, 0.8, 2.5 mM), the adsorption capacity of CaMgAl-900 was slightly greater, while at high concentrations (5–20 mM) its adsorption effect was lower (Figure 4c). These results indicated that borate concentration did affect

the adsorption effect of LDHs and Mg-doped LDHs with different calcination temperatures. In order to clarify the underlying mechanisms of these differences, the following characterizations were made.

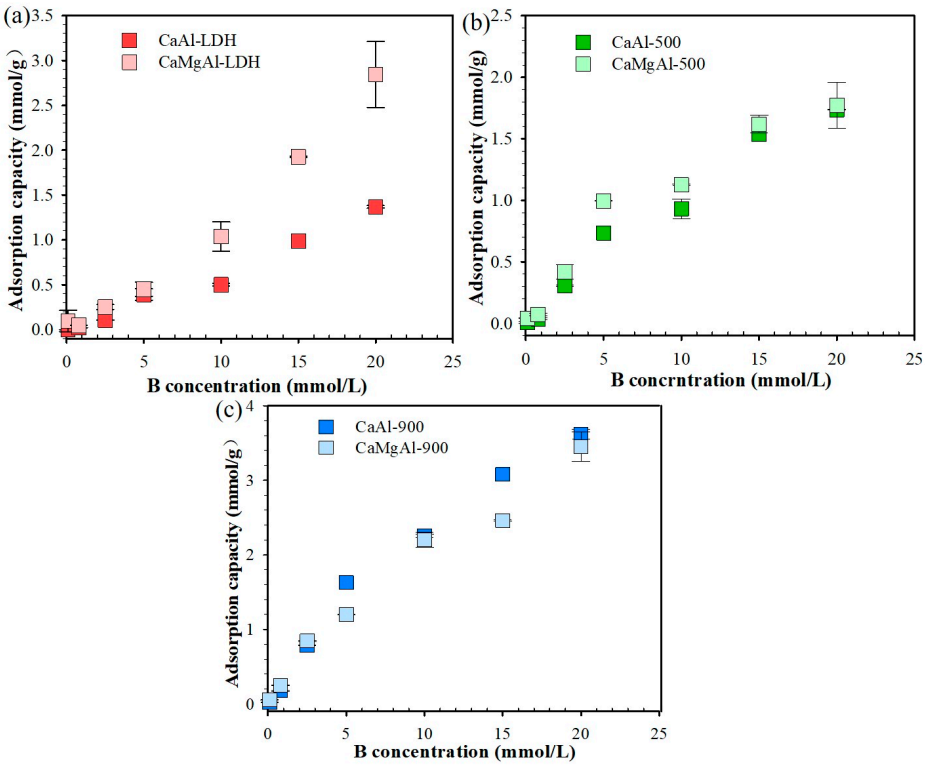

Figure 4. The equilibrium adsorption capacity after adsorption of different concentrations of borate. (**a**) CaAl-LDH and CaMgAl-LDH; (**b**) CaAl-500 and CaMgAl-500; (**c**) CaAl-900 and CaMgAl-900. Reaction time: 48 h.

3.2.2. XRD and SEM Analysis

The XRD patterns of CaAl-LDH and CaMgAl-LDH after adsorption of borate with different concentrations for 48 h were depicted in Figure 5. Notably, after adsorbing 0.8, 2.5, or 5 mM borate, two distinct types of CaAl-LDH with interlayer spacing of 8.67 Å and 7.56 Å were observed, indicating the existence of multiple interlayer anions [21]. As the borate concentration increased, the interlayer spacing of CaAl-LDH transformed into 8.23 Å and 7.56 Å, with the corresponding interlayer anions becoming $B(OH)_4^-$ and OH^- [11]. Unfortunately, the crystal phase of CaAl-LDH deteriorated under these conditions (Figure 5a). Conversely, the crystal phase of CaMgAl-LDH showed no significant differences after adsorption, except for a slight increase in interlayer spacing with increasing borate concentration (Figure 5b). Combined with the results of Figure 4a, it can be speculated that the diminished adsorption capacity of CaAl-LDH at higher borate concentrations may be due to its poorer crystal phase, suggesting that ion exchange may not be the primary adsorption mechanism.

Figure 6 presented the SEM images of the solid residues obtained after adsorption of 2.5 mM and 20 mM borate for 48 h. Compared with CaAl-LDH, no relatively regular and complete hexagonal structures were found in CaMgAl-LDH. After adsorption of low borate concentration (2.5 mM), their structure became incomplete, especially for CaMgAl-LDH (Figure 6e). However, at a borate concentration of 20 mM, the hexagonal flake structure appeared again. These findings could tentatively suggest that the borate concentration affected the morphology of LDHs after adsorption, while the doping of Mg exacerbated the deterioration of their morphology.

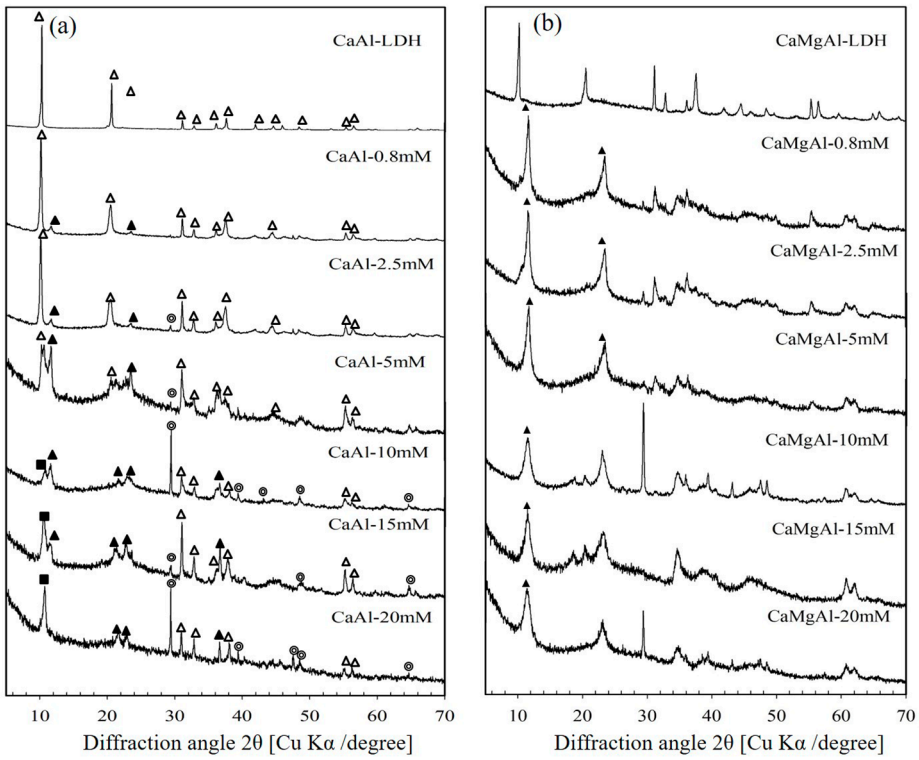

Figure 5. XRD patterns for the original CaAl-LDH and CaMgAl-LDH and their solid residues after adsorption of 0.80–20 mM B for 48 h. (**a**) CaAl-LDH, (**b**) CaMgAl-LDH. Symbols: △, Ca(Mg)Al-LDH (interlayer anion: NO_3^-); ▲, Ca(Mg)Al-LDH (interlayer anion: OH^-); ■, Ca(Mg)Al-LDH (interlayer anion: $B(OH)_4^-$); ◎, $CaCO_3$.

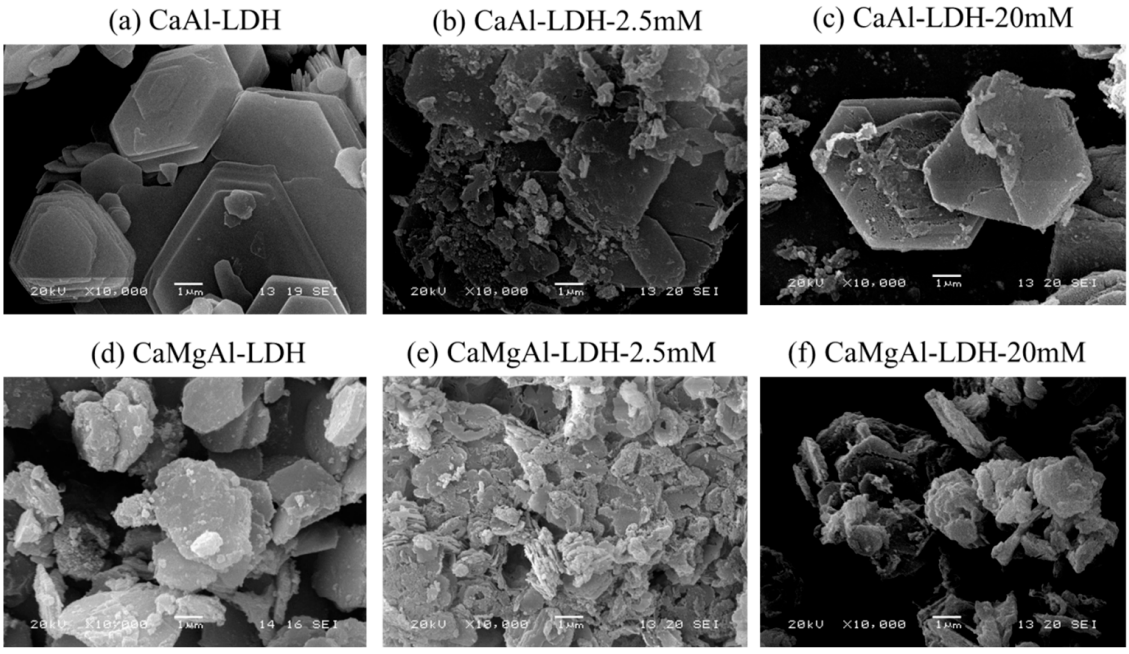

Figure 6. SEM images before and after adsorption of 2.5 mM and 20 mM borate for 48 h on CaAl-LDH and CaMgAl- LDH.

The XRD patterns of CaAl-500 and CaMgAl-500 after adsorbing different concentrations of borate for 48 h were shown in Figure 7. It is important to note that there were no discernible differences between the XRD results of CaAl-500 and CaMgAl-500. However, as

the borate concentration increased, the LDHs with an interlayer spacing of 7.42 Å gradually diminished, while the content of ettringite steadily increased. Interestingly, the content of LDHs in CaMgAl-500 started to decrease at a borate concentration of 5 mM, while in CaAl-500, this phenomenon occurred at a higher concentration of 10 mM. This trend suggests that higher concentrations of borate facilitate the formation of ettringite, and the presence of magnesium doping lowers the concentration of borate required for this reaction to occur. This could possibly explain the enhanced adsorption effect observed in CaMgAl-500 (Figure 4b).

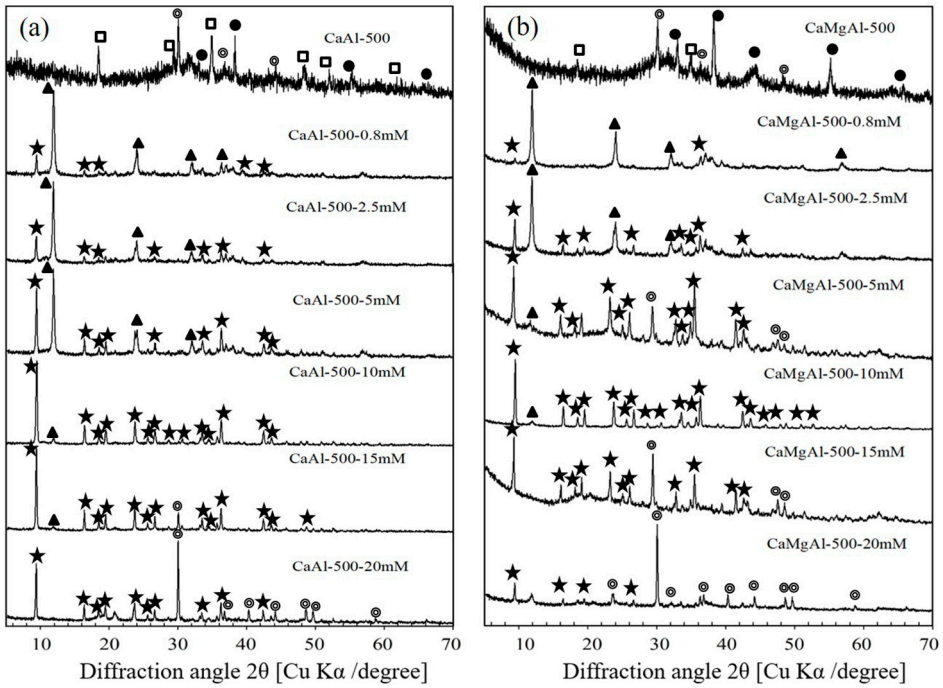

Figure 7. XRD patterns for the original CaAl-500 and CaMgAl-500 and their solid residues after adsorption of 0.80–20 mM B for 48 h. (**a**) CaAl-500, (**b**) CaMgAl-500. Symbols: ★, borate-containing ettringite ($Ca_6[Al(OH)_6]_2[B(OH)_4]_6$); ▲, Ca(Mg)Al-LDH (interlayer anion: OH^-); ◎, $CaCO_3$; □, $Ca(OH)_2$; ●, CaO.

Figure 8 displayed the SEM images of the solid residues obtained after adsorbing 2.5 mM and 20 mM borate using CaAl-500 and CaMgAl-500 for 48 h. The morphology of CaAl-500 and CaMgAl-500 was totally different. Remarkably, the morphology of CaAl-500 and CaMgAl-500 appeared distinct from each other. After adsorbing 2.5 mM borate, a rod-shaped structure, known as ettringite, was observed. However, at a higher borate concentration of 20 mM, the presence of rod-shaped structures was scarce in the CaMgAl-500 system, which is consistent with the XRD results (Figure 7).

The XRD patterns of CaAl-900 and CaMgAl-900 after reacting with different concentrations of borate for 48 h were presented in Figure 9. When reacted with 0.8 mM borate, the calcination products transformed into $Ca_3Al_2(OH)_{12}$ and LDHs with an interlayer spacing of 7.82 Å. As the borate concentrations increased, the content of $Ca_3Al_2(OH)_{12}$ gradually decreased and completely disappeared at a concentration of 10 mM borate. At this point, the interlayer spacing of the regenerated CaAl-LDH and CaMgAl-LDH was measured to be 8.16 Å, indicating the interlayer anion was $B(OH)_4^-$. However, the regenerated CaMgAl-LDH exhibited poor crystallinity, particularly at borate concentrations of 10 and 15 mM. Notably, at a borate concentration of 20 mM, ettringite appeared, and its relative content was higher in the CaMgAl-900-20 mM system. These results demonstrate that the concentration of borate has a significant impact on the composition of the reaction product, the doping of Mg influenced the crystallinity of the regenerated LDHs in high concentrations, resulting in lower adsorption effectiveness for CaMgAl-900 (Figure 4c).

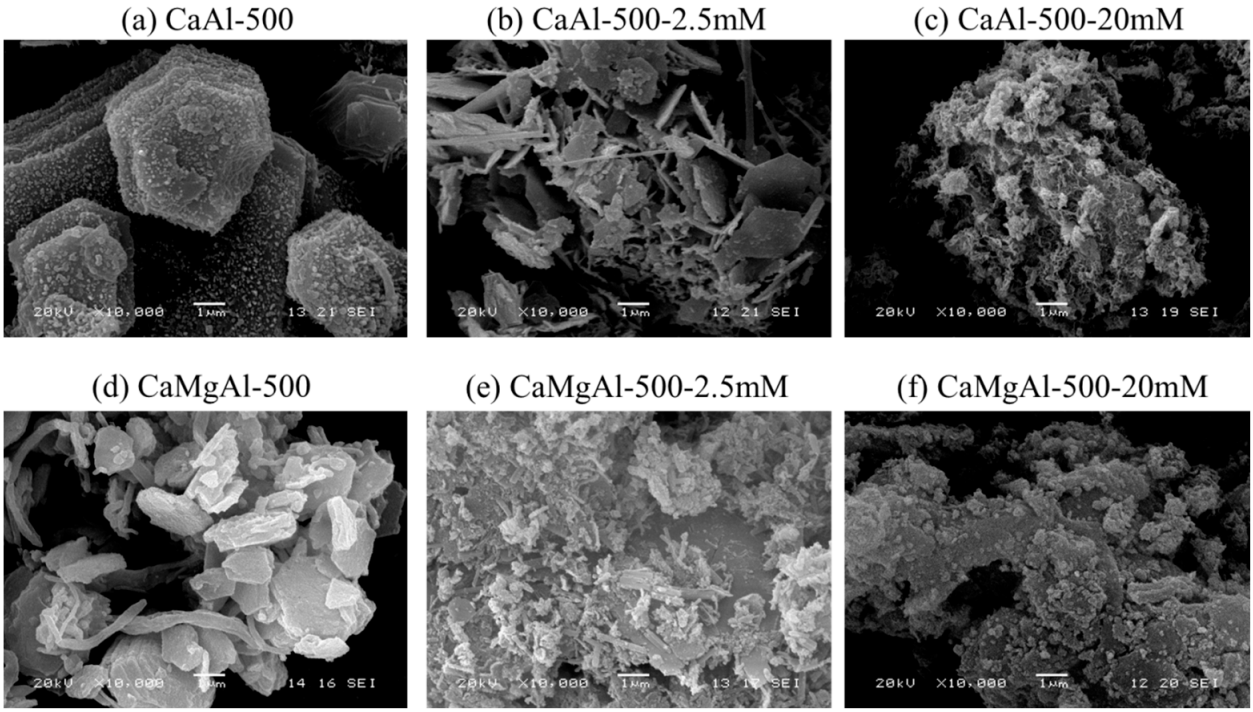

Figure 8. SEM images before and after adsorption of 2.5 mM and 20 mM borate for 48 h on CaAl-500 and CaMgAl-500.

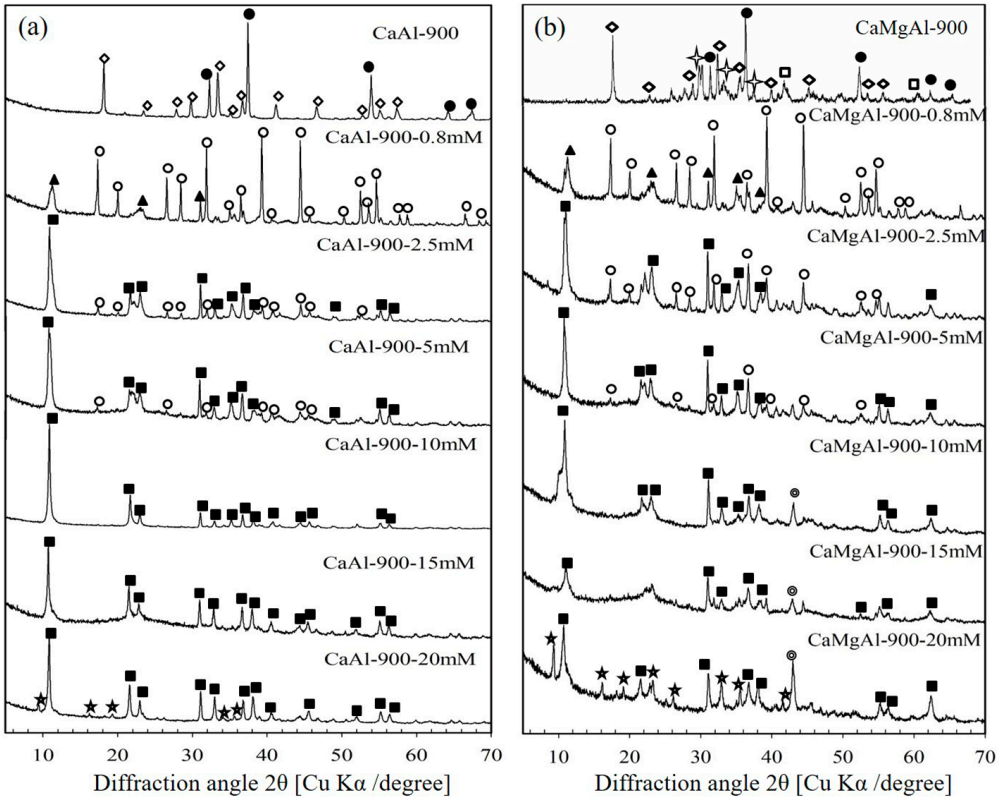

Figure 9. XRD patterns for the original CaAl-900 and CaMgAl-900 and their solid residues after adsorption of 0.80–20 mM B for 48 h. (**a**) CaAl-900, (**b**) CaMgAl-900. Symbols: ★, borate-containing ettringite ($Ca_6[Al(OH)_6]_2[B(OH)_4]_6$); ▲, Ca(Mg)Al-LDH (interlayer anion: OH^-); ■, Ca(Mg)Al-LDH (interlayer anion: $B(OH)_4^-$); ◎, $CaCO_3$; □, MgO; ●, CaO; ◇, $Ca_{12}Al_{14}O_{33}$; ○, $Ca_3Al_2(OH)_{12}$; ✧, $Ca_5Al_6O_{14}$.

The SEM images of the solid residues after adsorption of 2.5 mM and 20 mM borate for 48 h were presented in Figure 10. At low borate concentrations, there were no obvious differences (Figure 10b,e). However, the high borate concentration resulted in more fragmentation in the reaction product.

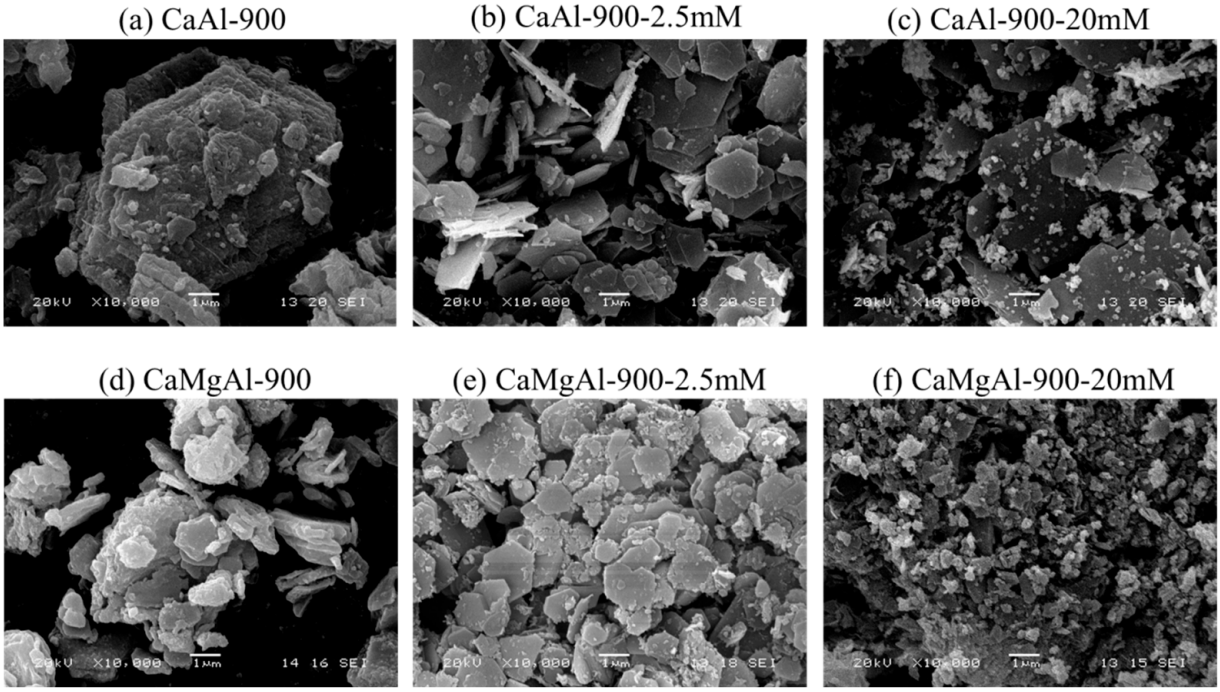

Figure 10. SEM images before and after adsorption of 2.5 mM and 20 mM borate for 48 h on CaAl-900 and CaMgAl-900.

4. Discussion

4.1. The Effect of Mg Doping

For uncalcined Ca-based LDHs, the adsorption mechanisms of borate involve the intercalation, dissolution-reprecipitation (DR) reaction and surface complexation. Among them, the DR process was attributed to the solubility of CaAl-LDH. So, the following dissolution occurred [36].

$$Ca_2Al(OH)_6 \cdot NO_3 \rightarrow 2Ca^{2+} + Al(OH)_4^- + 2OH^- + NO_3^- \quad (3)$$

In addition, the electrostatic potential (ESP) value for $B(OH)_4^-$ was −117.76 kcal/mol which was less negative than that of OH^- (−175.74 kcal/mol). This means that OH^- had a stronger affinity for the host layer of CaAl-LDH than $B(OH)_4^-$, making it easier to occupy the sorption sites of newly regenerated LDHs.

$$2Ca^{2+} + Al(OH)_4^- + 3OH^- \rightarrow Ca_2Al(OH)_6 \cdot OH \quad (4)$$

However, as a result of their layered structures, the DR mechanism was more prone to occur at the edges of the LDHs. The newly formed LDH ($Ca_2Al(OH)_6 \cdot OH$) appeared at the edge of the original LDHs and inhibited the further dissolution of $Ca_2Al(OH)_6 \cdot NO_3$ [21]. Thus, only a small amount of LDHs can dissolve, resulting in two types of LDHs (Figure 2). Simultaneously, owing to the affinity of $B(OH)_4^-$ being greater than NO_3^-, partial intercalation occurs. Besides, the positive charge of the laminated LDH sheets promoted the occurrence of surface adsorption.

In contrast, according to XRD results (Figure 2), OH^- was the only interlayer anion of new CaMgAl-LDH, indicating the doping of Mg facilitated the dissolution-reprecipitation process of CaMgAl-LDH. According to their SEM images after adsorption (Figure 6), there

were larger amounts of fragments that were caused by the dissolution-reprecipitation process in the CaMgAl-LDH system than in the CaAl-LDH system. In addition, CaMgAl-LDH had larger specific surface areas (Table S1), providing many more surface adsorption sites, so the final adsorption effect was better. For CaMgAl-LDH, the surface complexation became the predominant adsorption mechanism.

After calcination at 500 °C, the adsorption mechanism of borate was the formation of ettringite. During this process, the calcined LDHs were firstly hydrated to generate new LDHs with the interlayer anion of OH^-.

$$Ca_4Al_2O_5(OH)_4 + 5H_2O \rightarrow 2Ca_2Al(OH)_6 \cdot OH \quad (5)$$

Subsequently, the newly regenerated LDHs dissolved locally. But the dissolved species bound with $B(OH)_4^-$ to form borate-containing ettringite ($Ca_6[Al(OH)_6]_2[B(OH)_4]_6$), as borate ions had a higher tendency to form ettringite than other oxyanions [37,38].

$$6Ca^{2+} + 2Al(OH)_4^- + 6B(OH)_4^- + 3OH^- \rightarrow Ca_6[Al(OH)_6]_2[B(OH)_4]_6 \quad (6)$$

However, the doping of Mg had an impact on these processes. The regeneration process of MgAl-500 was significantly different from CaAl-500. For MgAl-500, hydration and ionization first happened on the surface, leading to the formation of ≡Mg-OH, ≡Al-OH, ≡Mg-OH_2^+, and ≡Al-OH_2^+ groups. $B(OH)_4^-$ was adsorbed onto these active groups by electrostatic interaction, and then immobilized inside the anionic layers of Mg-LDH [20]. Therefore, the regeneration rate of MgAl-500 was slower than CaAl-500. Although there was only a small amount of Mg in CaMgAl-500, it still inhibited the regeneration rate at the initial stage of the reaction. Because in the CaMgAl-500 system, the appearance of ettringite was slower (Figure 2). On the other hand, during the process of structural transformation (Equations (1) and (4)), considering the presence of Mg^{2+}, $Mg(OH)_2$ might be generated in an alkaline solution and further promote the transformation of ettringite. Some $B(OH)_4^-$ would be adsorbed by $Mg(OH)_2$. So, CaMgAl-500 had a better removal effect (Figure 1) and the reaction products presented a greater diffraction intensity (Figure 2).

As for the CaAl-900, which consists of $Ca_{12}Al_{14}O_{33}$ and CaO, the following hydration would occur in the aqueous phase [39,40].

$$Ca_{12}Al_{14}O_{33} + (48 + x)\ H_2O \rightarrow 6[Ca_2Al(OH)_6] \cdot [Al(OH)_4] + Al_2O_3 \cdot xH_2O \quad (7)$$

$$CaO + H_2O \rightarrow Ca(OH)_2 \quad (8)$$

$[Ca_2Al(OH)_6] \cdot [Al(OH)_4]$ would be slowly converted to the more stable $Ca_3Al_2(OH)_{12}$ (Figure 2). Boron species can be rapidly immobilized in Al_2O_3 and $Al(OH)_3$, due to $Al_2O_3 \cdot xH_2O$ being in a gel form. As the reaction progressed, the alumina gel was transformed to $Al(OH)_4^-$ under alkaline conditions. Then the boron species within the aluminum gel and OH^- in water can be immobilized as anions in the interlayer of LDHs [22,41].

$$x\ Ca(OH)_2 + Al(OH)_4^- + 3\ OH^- \rightleftarrows Ca_XAl(OH)_{2+2X} \cdot OH + 2\ OH^- \quad (9)$$

$$x\ Ca(OH)_2 + Al(OH)_4^- + B(OH)_4^- \rightleftarrows Ca_XAl(OH)_{2+2X} \cdot B(OH)_4 + 2\ OH^- \quad (10)$$

Furthermore, The boron species in CaAl-LDH also underwent a change from tetrahedral $B(OH)_4^-$ to trigonal HBO_3^{2-} [42].

$$2x\ Ca(OH)_2 + 2Al(OH)_4^- + B(OH)_4^- \rightarrow [Ca_XAl(OH)_{2+2X}]_2 \cdot HBO_3 + 2H_2O + 3OH^- \quad (11)$$

For Mg-doped LDHs, after calcination at 900 °C, its product consists of $Ca_{12}Al_{14}O_{33}$, CaO, MgO and other metal oxides that have not been accurately identified. The following reaction also occurred at pH > 12.

$$MgO + H_2O \rightarrow Mg(OH)_2 \quad (12)$$

In addition, inevitably, active groups (≡Mg-OH and ≡Mg-OH_2^+) may also be generated on the surface of metal oxides. The borate adsorbed on the surface by these groups would hinder the above reaction (Equations (7) and (8)). Therefore, the regeneration rate of CaMgAl-900 was reduced at the beginning of the reaction, and the crystallinity of the reaction product was also poor at that time (Figure 2).

4.2. The Effect of Initial Borate Concentration

For uncalcined LDHs, the dissolution-reprecipitation (DR) reaction obtained a certain inhibitory effect on the intercalation reaction but enhanced the surface adsorption of the borate. For CaMgAl-LDH, its more unstable structure results in the DR reaction occurring easier, which in turn, made surface adsorption the predominant adsorption mechanism for it. Therefore, under low borate concentrations, the adsorption capacity of borate on CaAl-LDH and CaMgAl-LDH was similar. The doping of Mg only altered the morphology of the reaction product and had little effect on their crystallinity. In contrast, at high borate concentrations, a large number of anions attached to the surface would inhibit the process of dissolution-reprecipitation, leading to the limitation of surface adsorption and ion exchange of CaAl-LDH. However, the interlayer spacing of CaMgAl-LDH under high borate concentrations was larger than that under low borate concentrations, indicating a part of attached $B(OH)_4^-$ could enter into the interlayer, resulting in a better adsorption effect. The illustration of the effect of borate concentration on the adsorption of CaAl-LDH and CaMgAl-LDH was summarized in Figure 11.

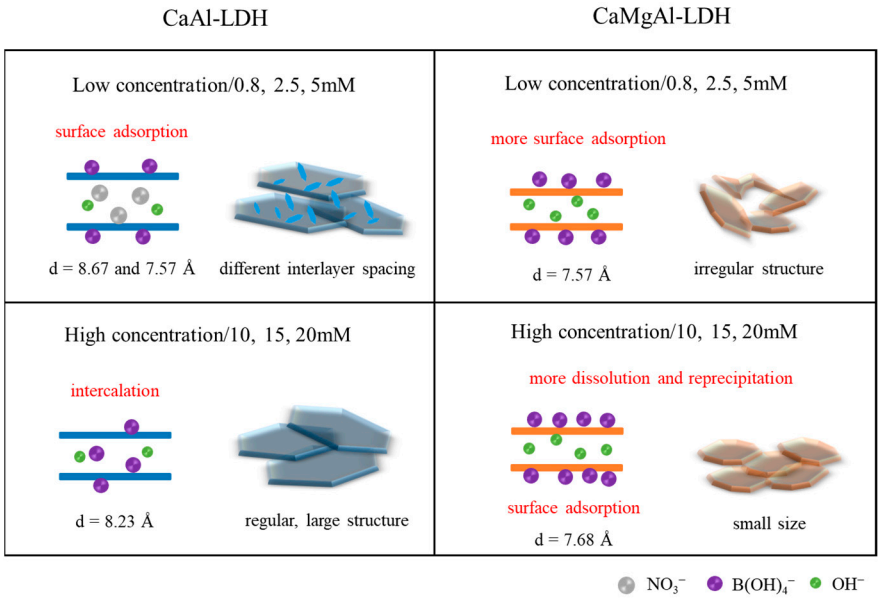

Figure 11. Schematic illustration to show the differences in adsorption of borate on CaAl-LDH and CaMgAl-LDH, depending on the concentrations.

The adsorption mechanism of borate on CaAl-500 and CaMgAl-500 was primarily through the ettringite formation. For CaAl-500, the initial borate concentration had no significant effect on adsorption behavior. However, as the borate concentration increases, the content of ettringite also increases significantly, resulting in structural agglomeration (Figure 8). Notably, Mg doping promoted the structure transformation of LDHs into ettringite at any borate concentration. However, the presence of Mg showed no apparent impact on the structure and morphology of the reaction product. The illustration for the borate concentrations dependent adsorption characteristics on CaAl-500 and CaMgAl-500 was illustrated in Figure 12.

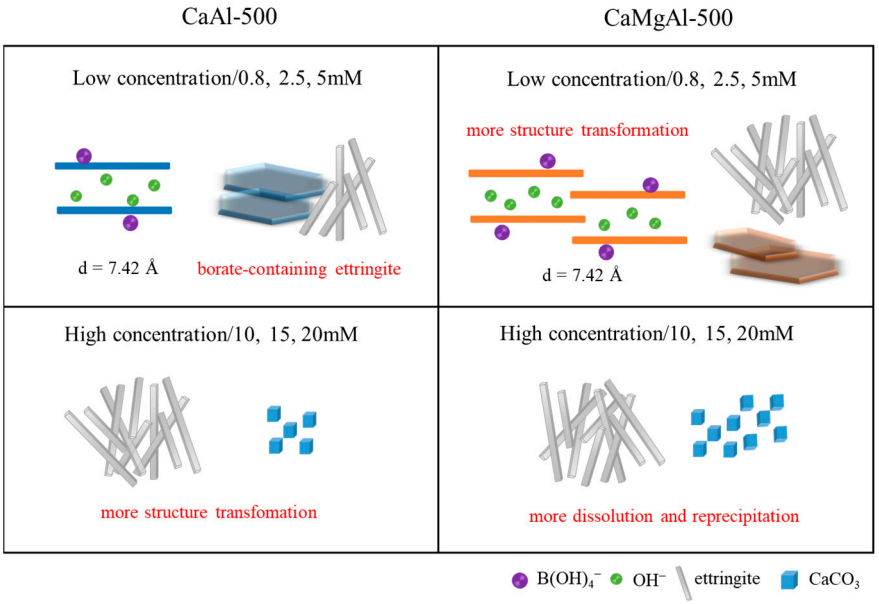

Figure 12. Schematic illustration to show the differences in adsorption of borate onto CaAl-500 and CaMgAl-500, depending on the concentrations.

The adsorption mechanism of borate on CaAl-900 and CaMgAl-900 involved the hydration of metal oxides, the regeneration of LDHs and the immobilization of borate. For CaAl-900, increasing the borate concentration only resulted in a more complete structure transformation of the metal oxides, without obvious effect on the crystallinity and morphology of the product. In contrast, the dissolution-reprecipitation reaction was more likely to occur due to regenerated CaMgAl-LDH being more unstable, especially at high borate concentrations. Besides, $B(OH)_4^-$ could accelerate the dissolution of LDHs by the strong affinity with Mg^{2+}, so the crystallinity and the flake structure of newly regenerated LDHs were obviously destroyed (Figures 9 and 10). The illustration of the effect of borate concentration on the adsorption of CaAl-900 and CaMgAl-900 is shown in Figure 13.

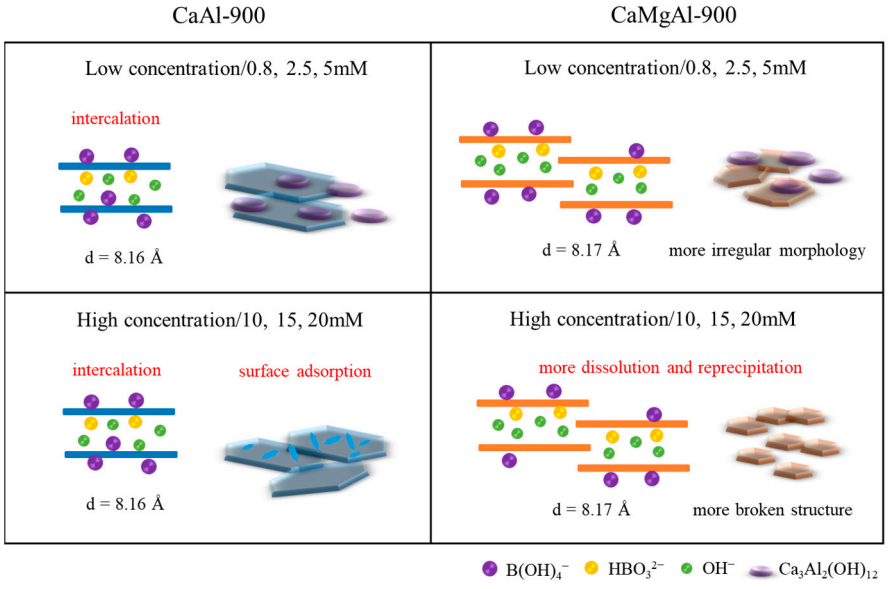

Figure 13. Schematic illustration to show the differences in adsorption of borate onto CaAl-900 and CaMgAl-900, depending on the concentrations.

5. Conclusions

The influence of Mg doping on borate adsorption by CaAl-LDH with varying calcination temperatures is investigated, along with the effect of initial borate concentrations on the adsorption behaviors of these materials.

During the adsorption of 2.5 mM borate, Mg doping increases the removal efficiency of CaAl-LDH but also affects the crystallinity and morphology of the product. The regeneration rate of CaAl-500 is initially slowed down, but ultimately facilitates the structural transformation of LDHs, resulting in better adsorption. The rehydration process of CaMgAl-900 is initially inhibited, but the larger BET surface area resulted in more efficient borate adsorption.

Under a wide range of borate concentrations, the crystallinity of CaAl-LDH is affected at high concentrations while the crystallinity of CaMgAl-LDH remains unaffected. The morphological structures of these materials are also affected differently by concentration. After calcination at 500 °C, high concentration is more conducive to ettringite formation, but Mg doping decreases this concentration, resulting in better adsorption for CaMgAl-500. Borate concentration does not have an obvious effect on the crystallinity and morphology of these materials. In contrast, the concentration affects the composition of the 900 °C calcined product. Due to the regeneration processes of CaAl-900 and CaMgAl-900 being different, Mg doping significantly inhibits the adsorption of CaAl-900. High borate concentration affects the crystallinity and morphology of the regenerated CaMgAl-LDH.

This study aims to enhance the understanding of borate adsorption behavior on Ca-based LDHs and Mg-doped Ca-based LDHs, as well as provide research guidance for other types of binary and corresponding ternary LDHs in natural systems.

Supplementary Materials: The following supporting information can be downloaded at: https://www.mdpi.com/article/10.3390/min13111398/s1, Test S1: Preparation of LDHs and calcined LDHs; Test S2: Characterization; Figure S1: Adsorption kinetics of borate by CaAl-LDH and CaMgAl-LDH with different calcination temperatures. (a) Pseudo-first-order kinetic mode (b) Pseudo-second-order kinetic mode; Figure S2: TG/DSC results of (a) CaAl-LDH and (b) CaMgAl-LDH. Reaction temperature is from room temperature to 1000 °C; Figure S3: N_2 adsorption–desorption isotherms of all adsorbents; Figure S4: FTIR spectra of solid residues after adsorption of 2.5 mM borate on CaAl-LDH and CaMgAl-LDH with different calcination temperatures; Table S1: Surface properties of different adsorbents.

Author Contributions: Conceptualization, S.X. and X.Q.; methodology, S.X., B.G. and X.Q.; software, S.X. and B.G.; data curation, S.X. and B.G.; writing—original draft preparation, S.X.; writing—review and editing, X.Q. and K.S.; visualization, B.G. and X.Q.; supervision, K.S. and X.Q.; funding acquisition, K.S. and X.Q. All authors have read and agreed to the published version of the manuscript.

Funding: This research was funded by National Science Foundation of China (51504170), and the Innovative Team program of Natural Science Foundation of Hubei Province (2021CFA032).

Data Availability Statement: The data presented in this study are available upon request from the corresponding author.

Acknowledgments: We are grateful to the editors and reviewers for their constructive comments and suggestions.

Conflicts of Interest: The authors declare no conflict of interest.

References

1. Yan, H.; Chen, Q.; Liu, J.; Feng, Y.; Shih, K. Phosphorus Recovery through Adsorption by Layered Double Hydroxide Nano-Composites and Transfer into a Struvite-like Fertilizer. *Water Res.* **2018**, *145*, 721–730. [CrossRef] [PubMed]
2. Borges, G.A.; Ferreira, G.M.D.; Siqueira, K.P.F.; Dias, A.; Navarro, K.O.N.; Silva, S.J.B.E.; Rodrigues, G.D.; Mageste, A.B. Adsorption of Organic and Inorganic Arsenic from Aqueous Solutions Using MgAl-LDH with Incorporated Nitroprusside. *J. Colloid Interface Sci.* **2020**, *575*, 194–205. [CrossRef] [PubMed]
3. Yang, L.; Chen, M.; Lu, Z.; Huang, Y.; Wang, J.; Lu, L.; Cheng, X. Synthesis of CaFeAl Layered Double Hydroxides 2D Nanosheets and the Adsorption Behaviour of Chloride in Simulated Marine Concrete. *Cem. Concr. Compos.* **2020**, *114*, 103817. [CrossRef]

4. Sonoyama, N.; Takagi, K.; Yoshida, S.; Ota, T.; Kimilita, P.D.; Ogasawara, Y. Optical Properties of the Europium (II) and (III) Ions Doped Metal Oxides Obtained from Sintering Layered Double Hydroxides, and Their Fine Structures. *Appl. Clay Sci.* **2020**, *186*, 105440. [CrossRef]
5. Jia, Y.; Wang, H.; Zhao, X.; Liu, X.; Wang, Y.; Fan, Q.; Zhou, J. Kinetics, Isotherms and Multiple Mechanisms of the Removal for Phosphate by Cl-Hydrocalumite. *Appl. Clay Sci.* **2016**, *129*, 116–121. [CrossRef]
6. Guo, Q.; Tian, J. Removal of Fluoride and Arsenate from Aqueous Solution by Hydrocalumite via Precipitation and Anion Exchange. *Chem. Eng. J.* **2013**, *231*, 121–131. [CrossRef]
7. Ma, B.; Fernandez-Martinez, A.; Grangeon, S.; Tournassat, C.; Findling, N.; Claret, F.; Koishi, A.; Marty, N.C.M.; Tisserand, D.; Bureau, S.; et al. Evidence of Multiple Sorption Modes in Layered Double Hydroxides Using Mo As Structural Probe. *Environ. Sci. Technol.* **2017**, *51*, 5531–5540. [CrossRef]
8. Zhu, J.; Zhu, Z.; Zhang, H.; Lu, H.; Qiu, Y.; Zhu, L.; Küppers, S. Enhanced Photocatalytic Activity of Ce-Doped Zn-Al Multi-Metal Oxide Composites Derived from Layered Double Hydroxide Precursors. *J. Colloid Interface Sci.* **2016**, *481*, 144–157. [CrossRef]
9. Wang, Y.; Dai, X.; Zhou, Q.; Li, K.; Feng, L.; Liao, W.; Yu, Y.; Yu, H.; Zong, X.; Lu, G.; et al. Insights into the Role of Metal Cation Substitution on the Anionic Dye Removal Performance of CoAl-LDH. *Colloids Surf. A Physicochem. Eng. Asp.* **2022**, *636*, 128139. [CrossRef]
10. Rybka, K.; Matusik, J.; Kuligiewicz, A.; Leiviskä, T.; Cempura, G. Surface Chemistry and Structure Evaluation of Mg/Al and Mg/Fe LDH Derived from Magnesite and Dolomite in Comparison to LDH Obtained from Chemicals. *Appl. Surf. Sci.* **2021**, *538*, 147923. [CrossRef]
11. Qiu, X.; Sasaki, K.; Hirajima, T.; Ideta, K.; Miyawaki, J. Temperature Effect on the Sorption of Borate by a Layered Double Hydroxide Prepared Using Dolomite as a Magnesium Source. *Chem. Eng. J.* **2013**, *225*, 664–672. [CrossRef]
12. Mao, N.; Zhou, C.H.; Keeling, J.; Fiore, S.; Zhang, H.; Chen, L.; Jin, G.C.; Zhu, T.T.; Tong, D.S.; Yu, W.H. Tracked Changes of Dolomite into Ca-Mg-Al Layered Double Hydroxide. *Appl. Clay Sci.* **2018**, *159*, 25–36. [CrossRef]
13. Izquierdo, M.; Querol, X. Leaching Behaviour of Elements from Coal Combustion Fly Ash: An Overview. *Int. J. Coal Geol.* **2012**, *94*, 54–66. [CrossRef]
14. Ito, R.; Dodbiba, G.; Fujita, T.; Ahn, J.W. Removal of Insoluble Chloride from Bottom Ash for Recycling. *Waste Manag.* **2008**, *28*, 1317–1323. [CrossRef] [PubMed]
15. Grishchenko, R.O.; Emelina, A.L.; Makarov, P.Y. Thermodynamic Properties and Thermal Behavior of Friedel's Salt. *Thermochim. Acta* **2013**, *570*, 74–79. [CrossRef]
16. Ashekuzzaman, S.M.; Jiang, J.Q. Study on the Sorption-Desorption-Regeneration Performance of Ca-, Mg- and CaMg-Based Layered Double Hydroxides for Removing Phosphate from Water. *Chem. Eng. J.* **2014**, *246*, 97–105. [CrossRef]
17. Takaki, Y.; Qiu, X.; Hirajima, T.; Sasaki, K. Removal Mechanism of Arsenate by Bimetallic and Trimetallic Hydrocalumites Depending on Arsenate Concentration. *Appl. Clay Sci.* **2016**, *134*, 26–33. [CrossRef]
18. Gidado, S.M.; Akanyeti, İ. Comparison of Remazol Brilliant Blue Reactive Adsorption on Pristine and Calcined ZnAl, MgAl, ZnMgAl Layered Double Hydroxides. *Water. Air. Soil Pollut.* **2020**, *231*, 146. [CrossRef]
19. Theiss, F.L.; Ayoko, G.A.; Frost, R.L. Removal of Boron Species by Layered Double Hydroxides: A Review. *J. Colloid Interface Sci.* **2013**, *402*, 114–121. [CrossRef]
20. Qiu, X.; Sasaki, K.; Osseo-Asare, K.; Hirajima, T.; Ideta, K.; Miyawaki, J. Sorption of $H_3BO_3/B(OH)_4^-$ on Calcined LDHs Including Different Divalent Metals. *J. Colloid Interface Sci.* **2015**, *445*, 183–194. [CrossRef]
21. Xu, S.; Zhao, J.; Yu, Q.; Qiu, X.; Sasaki, K. Understanding How Specific Functional Groups in Humic Acid Affect the Sorption Mechanisms of Different Calcinated Layered Double Hydroxides. *Chem. Eng. J.* **2020**, *392*, 123633. [CrossRef]
22. Zhang, S.; Chen, Y.; Li, J.; Li, Y.; Song, W.; Li, X.; Yan, L.; Yu, H. Highly Efficient Removal of Aqueous Cu(II) and Cd(II) by Hydrothermal Synthesized CaAl-Layered Double Hydroxide. *Colloids Surf. A Physicochem. Eng. Asp.* **2022**, *641*, 128584. [CrossRef]
23. Tian, J.; Guo, Q.; Tian, J.; Guo, Q. Thermal decomposition of hydrocalumite over a temperature range of 400 °C–1500 °C and its structure reconstruction in water. *J. Chem.* **2014**, *2014*, e454098. [CrossRef]
24. Renaudin, G.; Humbert, B. Thermal Behaviour of the Nitrated AFm Phase $Ca_4Al_2(OH)_{12}(NO_3)_2 \bullet 4H_2O$ and Structure Determination of the Intermediate Hydrate $Ca_4Al_2(OH)_{12}(NO_3)_2 \bullet 2H_2O$. *Cem. Concr. Res.* **2000**, *30*, 307–314. [CrossRef]
25. Fukuda, H.; Tsuchiya, K.; Toba, Y.; Eguchi, M.; Tokoro, C. Rapid Boron Removal from Wastewater Using Low-Crystalline Magnesium Oxide. *J. Environ. Chem. Eng.* **2020**, *8*, 104171. [CrossRef]
26. Rahaman, S.H.; Bhattacharjee, A.; Saha, S.; Chakraborty, M.; Chakraborty, J. ShRNA Intercalation in CaAl-LDH Nanoparticle Synthesized at Two Different PH Conditions and Its Comparative Evaluation. *Appl. Clay Sci.* **2019**, *171*, 57–64. [CrossRef]
27. Zhou, J.Z.; Xu, Z.P.; Qiao, S.; Liu, J.; Liu, Q.; Xu, Y.; Zhang, J.; Qian, G. Triphosphate Removal Processes over Ternary CaMgAl-Layered Double Hydroxides. *Appl. Clay Sci.* **2011**, *54*, 196–201. [CrossRef]
28. Zhao, J.; Deng, L.; Zheng, W.; Xu, S.; Yu, Q.; Qiu, X. Nickel-Induced Structure Transformation in Hydrocalumite for Enhanced Ammonia Decomposition. *Int. J. Hydrog. Energy* **2020**, *45*, 12244–12255. [CrossRef]
29. Kim, T.H.; Heo, I.; Paek, S.M.; Park, C.B.; Choi, A.J.; Lee, S.H.; Choy, J.H.; Oh, J.M. Layered Metal Hydroxides Containing Calcium and Their Structural Analysis. *Bull. Korean Chem. Soc.* **2012**, *33*, 1845–1850. [CrossRef]
30. Zheng, L.; Bing, W.; Wang, H.; Zheng, L.; Rao, D.; Yang, Y.; Wang, B.; Wang, Y.; Wei, M. A CaMnAl-Hydrotalcite Solid Basic Catalyst toward the Aldol Condensation Reaction with a Comparable Level to Liquid Alkali Catalysts. *Green Chem.* **2018**, *20*, 3071–3080. [CrossRef]

31. Bing, W.; Zheng, L.; He, S.; Rao, D.; Xu, M.; Zheng, L.; Wang, B.; Wang, Y.; Wei, M. Insights on Active Sites of CaAl-Hydrotalcite as a High-Performance Solid Base Catalyst toward Aldol Condensation. *ACS Catal.* **2018**, *8*, 656–664. [CrossRef]
32. Bonometti, R.J. Destructive Interference Revisited. *Phys. Teach.* **1983**, *21*, 214. [CrossRef]
33. Zhang, P.; Qian, G.; Shi, H.; Ruan, X.; Yang, J.; Frost, R.L. Mechanism of Interaction of Hydrocalumites (Ca/Al-LDH) with Methyl Orange and Acidic Scarlet GR. *J. Colloid Interface Sci.* **2012**, *365*, 110–116. [CrossRef] [PubMed]
34. Qiu, X.; Sasaki, K.; Takaki, Y.; Hirajima, T.; Ideta, K.; Miyawaki, J. Mechanism of Boron Uptake by Hydrocalumite Calcined at Different Temperatures. *J. Hazard. Mater.* **2015**, *287*, 268–277. [CrossRef] [PubMed]
35. Luengo, C.V.; Volpe, M.A.; Avena, M.J. High Sorption of Phosphate on Mg-Al Layered Double Hydroxides: Kinetics and Equilibrium. *J. Environ. Chem. Eng.* **2017**, *5*, 4656–4662. [CrossRef]
36. Qian, G.; Feng, L.; Zhou, J.Z.; Xu, Y.; Liu, J.; Zhang, J.; Xu, Z.P. Solubility Product (Ksp)-Controlled Removal of Chromate and Phosphate by Hydrocalumite. *Chem. Eng. J.* **2012**, *181–182*, 251–258. [CrossRef]
37. Hiraga, Y.; Shigemoto, N. Boron uptake behavior during ettringite synthesis in the presence of H_3BO_3 and in a suspension of ettringite in H_3BO_3. *J. Chem. Eng. Jpn.* **2010**, *43*, 865–871. [CrossRef]
38. Chrysochoou, M.; Dermatas, D. Evaluation of ettringite and hydrocalumite formation for heavy metal immobilization: Literature review and experimental study. *J. Hazard. Mater.* **2006**, *136*, 20–33. [CrossRef]
39. Ukrainczyk, N.; Matusinovic, T.; Kurajica, S.; Zimmermann, B.; Sipusic, J. Dehydration of a layered double hydroxide-C_2AH_8. *Thermochim. Acta* **2007**, *464*, 7–15. [CrossRef]
40. Edmonds, R.N.; Majumdar, A.J. The hydration of $12CaO{\bullet}7Al_2O_3$ at different temperatures. *Cem. Concr. Res.* **1988**, *18*, 473–478. [CrossRef]
41. Zhi, P.X.; Guo, Q.L. Hydrothermal synthesis of layered double hydroxides (LDHs) from mixed MgO and Al_2O_3: LDH formation mechanism. *Chem. Mater.* **2005**, *17*, 1055–1062. [CrossRef]
42. Zhang, M.; Reardon, E.J. Removal of B, Cr, Mo, and Se from Wastewater by Incorporation into Hydrocalumite and Ettringite. *Environ. Sci. Technol.* **2003**, *37*, 2947–2952. [CrossRef] [PubMed]